Experimental Demonstration of a Solar Powered High Temperature Latent Heat Storage Prototype

Preliminary Results of an Experimental Validation Campaign

Asem Alemam[1] , Nicolas Lopez Ferber[1] , Tommy Malm[1] ,
Valerie Eveloy[1,2] , and Nicolas Calvet[1,3,*]

[1] Masdar Institute Solar Platform, Nuclear and Mechanical Engineering Department, Khalifa University

[2] Abu Dhabi Virtual Research Institute (VRI) on Sustainable Energy Production, Storage and Utilization, Khalifa University

[3] Research and Innovation Center on CO2 and Hydrogen (RICH), Nuclear and Mechanical Engineering Department, Khalifa University

Abstract. The challenge of imbalances between renewable energy supply and grid demand underscores the significance of energy storage in microgrids. This research presents an empirical assessment of the operational capabilities of a full-scale Electrical Thermal Energy Storage (ETES) prototype system named Thermal Energy Storage Power On Demand (TES.POD®), in solar-abundant and harsh desert conditions. The system incorporates a high-temperature commercial-scale latent heat thermal energy storage, integrated with a Stirling engine. Over a continuous span of 10 days, from September 26th to October 6th, 2022, the input and output power, as well as the heat transfer fluid temperatures during charging and discharging were monitored to assess the power block and system efficiencies. Results from the experiments reveal that this prototype effectively maintains a near-constant electricity production rate of 10.5 ± 1 kW for a discharge duration of 13 hours. Average cycle efficiency stands at 23%, while power block efficiency reaches 25%. These findings collectively suggest the system's potential for applications involving long duration thermal energy storage.

Keywords: Latent Heat Energy Storage, Electrical Thermal Energy Storage, Phase Change Material

1. Introduction

In spite of the cost efficiency advancements in solar energy technologies, significant challenges persist on both utility grid and microgrid levels. On the grid-scale, exemplified by California, the extensive deployment of solar PV has transformed the typical electricity demand curve into the "duck curve," posing risks of over-generation and fast ramp-up of demand at sunset coinciding with a fast decline of PV production [1].

Conversely, microgrids grapple with stability and flexibility issues. In grids and microgrids heavily reliant on PV, limited daytime solar availability and the solar resource's vulnerability to weather fluctuations contribute to supply-demand mismatches [2].

Long duration energy storage (LDES) systems hold promise for bolstering microgrid stability and flexibility, and are defined by their ability to discharge energy at nominal power for

1

8 hours or more [3]. It is anticipated that LDES systems capacity could reach up to 8 TWh by 2030 and 140 TWh by 2040 globally [4]. Given this projected growth, comprehensive exploration of LDES systems performance becomes essential.

Thermal energy storage (TES) techniques, encompassing sensible heat storage (SHS), latent heat storage (LHS), and thermochemical storage, can serve as LDES systems [5]. LHS offers advantages due to higher storage density and consistent temperature storage as they employ Phase Change Materials (PCMs) which transition between phases through heat addition or subtraction, occurring theoretically at a constant temperature [6]. Typically, solid-liquid PCMs are preferred due to their minimal volume change, ease of handling, and compactness [7], [8]. These PCMs are categorized by melting temperature—low (<40°C), medium (40°C-300°C), and high (>300°C) [9].

Thermal conductivity is recognized as a critical thermophysical property affecting LHS system design and efficacy [10]. High thermal conductivity PCMs streamline heat exchanger design and enable rapid heat storage/release with low temperature gradients [11], [12]. Unlike low thermal conductivity PCMs which require heat transfer enhancements like fins [13], encapsulation [14], nanoparticles [15], and graphite additives [16], high thermal conductivity PCMs negate the need for intricate designs. As a consequence, the available literature investigates metallic PCMs (especially aluminum alloys [17], [18]) as an alternative to nitrate, fluoride or chloride salts [19], [20], [21]. The transfer of heat to and from the PCM can also pose challenges, especially in regards to reliability and scalability, with potential issues of heat and mass transfer with sodium pool boilers or sodium vapor heat pipes.

Azelio AB (Sweden) has developed an ETES LHS system utilizing an 88Al-12Si metallic alloy as the PCM, paired with liquid sodium as the Heat Transfer Fluid (HTF) and a stirling engine using either hydrogen or helium as its working gas. This study involves the real-world experimental evaluation of prototypes, most notably in regards to their efficiency.

2. Objectives of the study

This work aims to evaluate the performance of a full-size prototype TES.POD® unit under realistic conditions at the Khalifa University's Masdar Institute Solar Platform (KUMISP). Up to the authors' knowledge, this is the first experimental report on dispatchable commercial-sized high temperature latent heat thermal energy storage. Data extracted from the TES.POD® at KUMISP is used to analyze the system performance in the light of:

- Energy input and output to and from the TES.POD®,
- HTF temperature profile during charge and discharge cycles,
- Power block efficiency, and
- TES.POD® cycle efficiency.

3. System description

Two prototypes TES.POD® units have been installed at the Khalifa University's Masdar Institute Solar Platform for a testing campaign in realistic conditions. During the charging phase, these units are supplied with electricity from either the grid or a 450 kWp solar PV field.

3.1 TES.POD® overview

Each TES.POD® unit comprises four key components: (i) the heating system, (ii) the PCM TES tank, (iii) two HTF loops for charging and discharging, and (iv) the power block. The heating system employs a 100 kW electric resistive heater to heat the HTF (liquid sodium). This heated HTF then transfers thermal energy, melting the Al-Si alloy within the PCM storage tank. During discharge, another HTF loop collects heat from the PCM tank and conveys it to

the power block's working fluid (hydrogen or helium) through a heat exchanger, referred to as *"gas heater"* in this work. The power block incorporates a Stirling engine that converts heat to electricity. Figure 1 illustrates a simplified schematic of the TES.POD®, outlining major components along with charge and discharge loops.
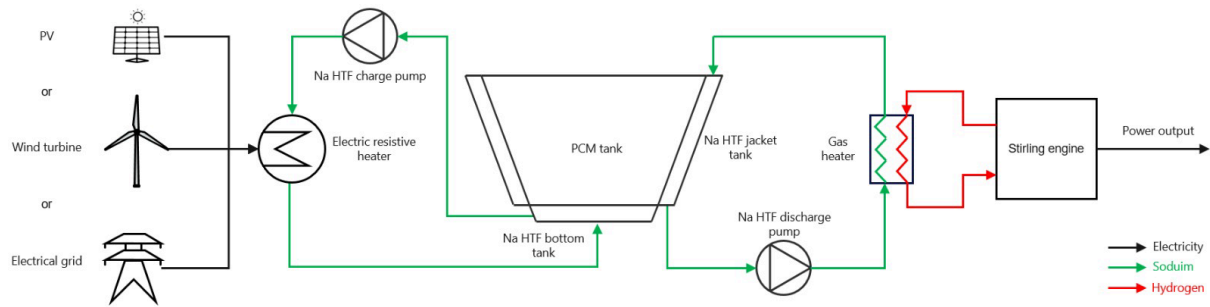
Figure 1. Simplified schematic diagram of Azelio's TES.POD® system

The choice of the 88Al-12Si eutectic alloy as the storage medium is primarily driven by its advantageous thermophysical properties, including high thermal conductivity, specific heat, and melting point. These attributes render it well-suited for electricity generation through a Stirling engine. Key characteristics and thermophysical properties of 88Al-12Si are summarized in Table 1. Each TES.POD® unit incorporates approximately 4,370 kg of PCM, providing a storage capacity of 600 kWh$_{th}$ [22].

To prevent corrosion, the PCM storage tank is constructed from Boron-Nitride-coated stainless steel, a technique demonstrated in a prior collaboration between Azelio and Khalifa University [23]. Perlite thermal insulation is employed to minimize heat losses.

Table 1. Summary of 88Al-12Si properties as a PCM in the temperature range of 500–750 ˚C

Property	Value	Reference
Density [kg.m^{-3}]	2653-2686	[24]
Melting point [˚C]	576	[25]
Liquid thermal conductivity [W.m^{-1}.K^{-1}]	70	[26]
Solid thermal conductivity [W.m^{-1}.K^{-1}]	181	[26]
Latent heat of fusion [kJ.kg^{-1}]	500	[23]
Liquid specific heat [kJ.kg^{-1}.K^{-1}]	1.64	[25]
Solid specific heat [kJ.kg^{-1}.K^{-1}]	1.04	[25]

The choice of sodium as the heat transfer fluid (HTF) in the TES.POD® system was motivated by its distinct advantages compared to alternatives like lead, lead-bismuth and Solar Salt within the system's operational temperature range. Liquid sodium is a high specific heat, high thermal conductivity, low viscosity fluid, with a low freezing temperature (which reduces the risk of solidifying in pipes during idle periods). Table 2 provides an insight into the thermophysical properties of some liquid metals that can serve as HTF within the operating temperature range of the TES.POD® (between 510 and 640˚C). Flow rates of the HTF during charge and discharge operations are approximately 3.2 and 1.62 [kg.s^{-1}], respectively.

Table 2. Thermophysical properties of possible liquid metal HTFs at 576˚C [27]

Property	Lead	Bismuth	Lead-bismuth	Sodium
Melting point [˚C]	327	271	125	98
Specific heat [kJ.kg^{-1}.K^{-1}]	0.144	0.132	0.139	1.256
Dynamic viscosity 10^{-3} [Pa.s]	1.6	1.12	1.25	0.21
Thermal conductivity [W.m^{-1}.K^{-1}]	18.8	15.3	15	63.2

4. Method and analysis

4.1 Data acquisition

To comprehensively monitor the TES.POD® performance, over 240 sensors are strategically positioned within the system. These sensors collect a range of data including pressure, engine speed, and temperature. This study particularly focuses on data obtained from N-type thermocouples temperature sensors, which possess an accuracy of ± 2.5˚C. These sensors are integrated into the HTF charge and discharge loops, upstream and downstream of the electric heater and the gas heater, respectively (Figure 2). During the charge phase, the primary monitored values are the input power to the electric heater and the charge HTF temperatures. On the other hand, the discharge phase entails the monitoring of the discharge HTF temperatures and the inverter power output of the Stirling engine.
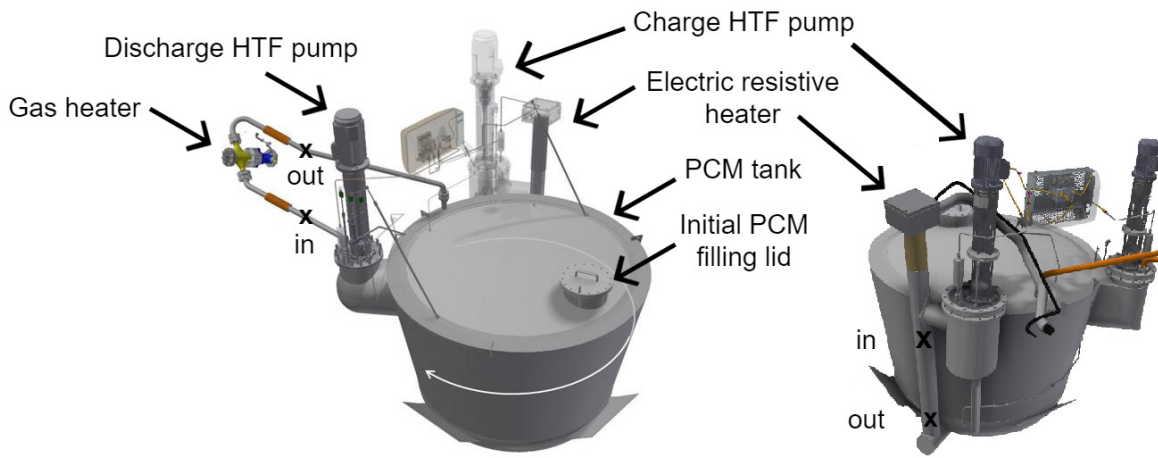
Figure 2 *Tank and HTF loops CAD drawing showing some of the main components and temperature sensors locations*

4.2 Experimental quantities

Experimental quantities are defined as follows:

- $E_{net,in}$, the sum of the electrical consumptions of the heater and the charge auxiliaries, during a charge.
- $E_{net,out}$, the electrical production at the outlet of the engine's inverter, minus the consumption of the discharge auxiliaries, during a discharge.
- $Q_{out,dis}$, the thermal flow from the discharge HTF loop to the gas heater, upstream from the stirling engine, during a discharge.

4.3 Key performance indicators

When it comes to the power block, its performance is evaluated based on the heat-to-electricity efficiency. The efficiency of the TES.POD®'s power block is given by:

$$\eta_{power\ block} = E_{net,out} / Q_{out,dis} \tag{1}$$

While the system efficiency, for each cycle, is defined as the ratio of electricity produced during the discharge phase to the electricity supplied during the charging phase.

$$\eta_{cycle} = E_{net,out} / E_{net,in} \tag{2}$$

5. Experimental results

This section details the experimental data obtained from the TES.POD® unit for 10 consecutive days from Sep. 26th to Oct. 6th, 2022 at the KUMISP. The time scale is in days, where the day begins in the first testing period at 9:00 and ends at 8:59 the next day. The 10-day test period is reported to demonstrate the performance of the TES.POD® for several charge and discharge scenarios.

5.1 Operation scenario

The TES.POD® operates in three distinct modes: charge, discharge, and idle. Table 3 provides insight into the durations of these operation modes across a span of 10 consecutive days, from September 26th to October 6th, 2022, at the KUMISP facility. The variations in daily durations arise from different testing patterns employed during this period. The average durations for charge, discharge, and idle modes throughout the testing phase are 6.8, 13.1, and 4.1 hours, respectively. Among these days, day 4 exhibits the shortest durations for both charge and discharge modes. Conversely, the longest discharge duration is observed on day 9, while days 3 and 5 had the longest charge duration.

Table 3. *TES.POD®'s operation modes duration from 10 consecutive days from Sep. 26th to Oct. 6th, 2022, at the KUMISP*

Day	Charge (hours)	Discharge (hours)	Idle (hours)
1	7.5	13	3.5
2	6	13	5
3	8	13	3
4	5	10	9
5	8	14	2
6	7	13	4
7	6.3	13	4.7
8	6	13	5
9	7	15	2
10	7	14	3
Average	6.8	13.1	4.1

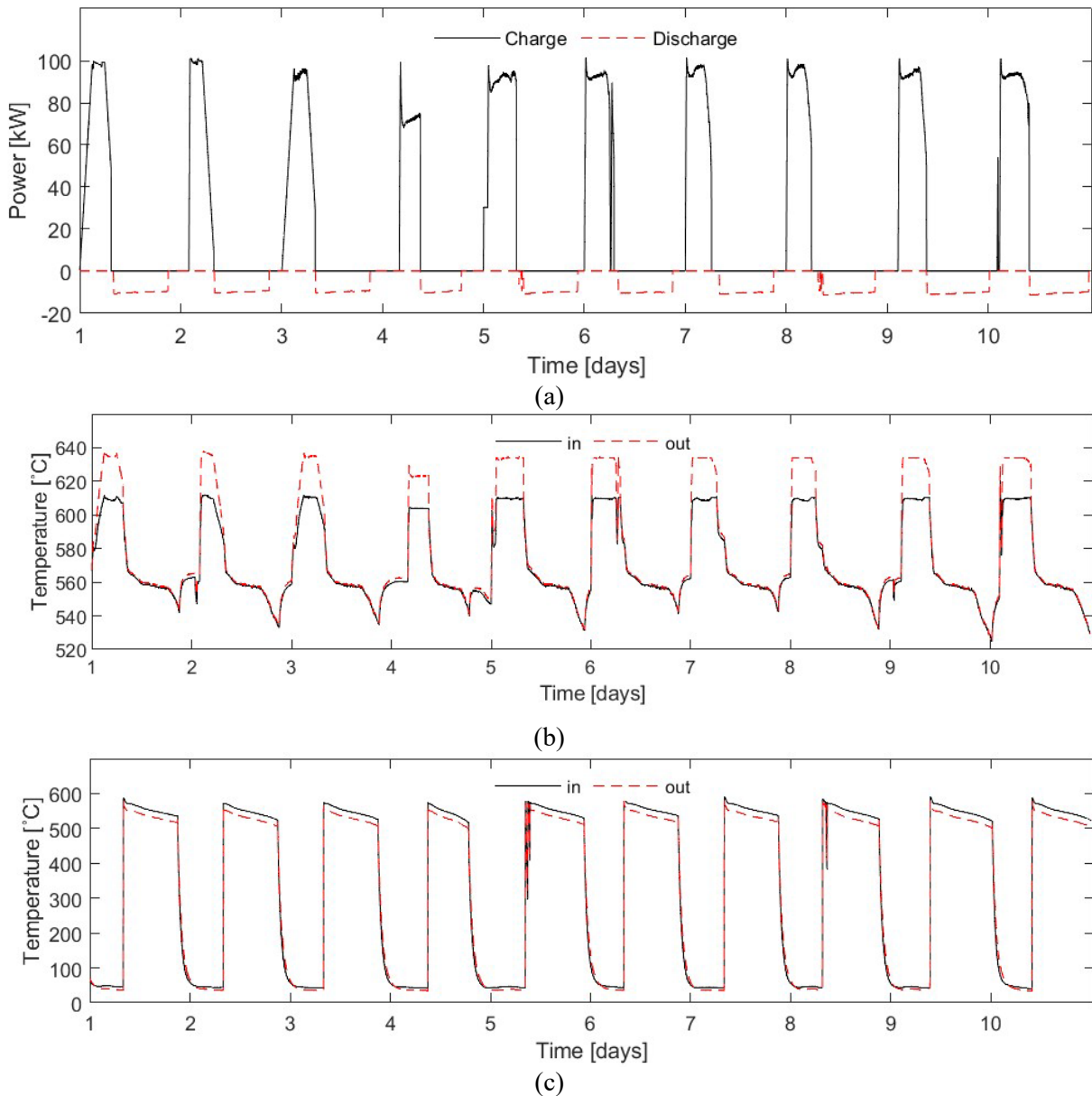### 5.2 Experimental measurements

A selection of experimental measurements collected from the TES.POD® unit at KUMISP is presented in Figure 3. These measurements encompass metrics such as gross power consumption during charge, gross power generation during discharge, inlet and outlet HTF temperatures of the heating element, and gas heater conditions. The discharge process across the test days yields an output power ranging between 9.5 and 11.5 kW. The electrical output attains its peak at the initial discharge cycle stages, gradually decreasing due to the decline in discharge HTF temperature. For the first 7 days, the Stirling engine operated at 1800 rpm and 125 bar, while the last 3 days see nominal power conditions at 1950 rpm and 125 bar. These operational variations lead to output power fluctuations, ranging from 9.5 to 11 kW during the initial 7 days and 10 to 11.5 kW afterwards. The deepest discharge happened on day 9, extending for 15 hours.

Figure 3 (b) illustrates the charge HTF temperature profile at the inlet and exit of the electric resistive heater. During charging, the heating element elevates the HTF temperature to around 635˚C, significantly exceeding the PCM's melting temperature to facilitate heat transfer towards the PCM tank. The heated HTF cycles through the bottom tank and returns

to the heater inlet at 610°C. The temperature difference between the outlet and return sections during charging enables the calculation of heat stored in the PCM.

Figure 3 (c) depicts the discharge HTF temperature profile at the gas heater's inlet and outlet. At the beginning of the discharge, HTF enters the gas heater at 570 to 590°C, dependent on final PCM temperature post-charge. Over 13 hours of operation, the discharge HTF temperature at the gas heater inlet slightly declines by 45 to 50°C due to continuous heat extraction from the PCM tank, resulting in reduced output power. By discharge cycle completion, the HTF temperature at the gas heater inlet is typically between 520 and 530°C. A consistent 20°C decrease in discharge HTF temperature occurs during its passage through the gas heater.

During discharge, the Stirling engine releases low-temperature waste heat to the ambient, functioning as the heat sink, at a rate spanning 20 to 23 kWth.

(a)

(b)

(c)

***Figure 3.** Experimental measurements from one TES.POD® during 10 consecutive days from Sep. 26th to Oct. 6th 2022 showing (a) the Power flow (b) the HTF temperature profiles across the heating element during charge phase and (c) the HTF temperature profiles across the gas heater in the discharge phase*

5.3 Performance indicators

Although Azelio's Stirling engine demonstrated a heat-to-mechanical work efficiency of 30% in a previous work [28], the TES.POD®'s power block tested in this work consistently exhibited heat-to-electricity net efficiency of 25% (Figure 4). The power block efficiency is impacted by the engine speed. It can be seen that when the engine speed is increased from 1800 rpm to 1950 rpm on days 8-10, its efficiency marginally dropped below the average value. This observation matches the parametric study results in Nilsson et al. [28]. Moreover, the Stirling engine efficiency featured an instantaneous efficiency of 26% at the beginning of the discharge with slight decrease with time until it reaches 24% after 13 hours of discharge. This near constant engine efficiency, which is mainly attributed to the highly conductive Al-Si alloy PCM, shows superior storage discharge performance compared to the salt-based PCM presented by White et al. [20], where the engine efficiency reduced from 25 to 5% within 2 hours due to the extremely low thermal conductivity of the NaF-NaCl salt used.
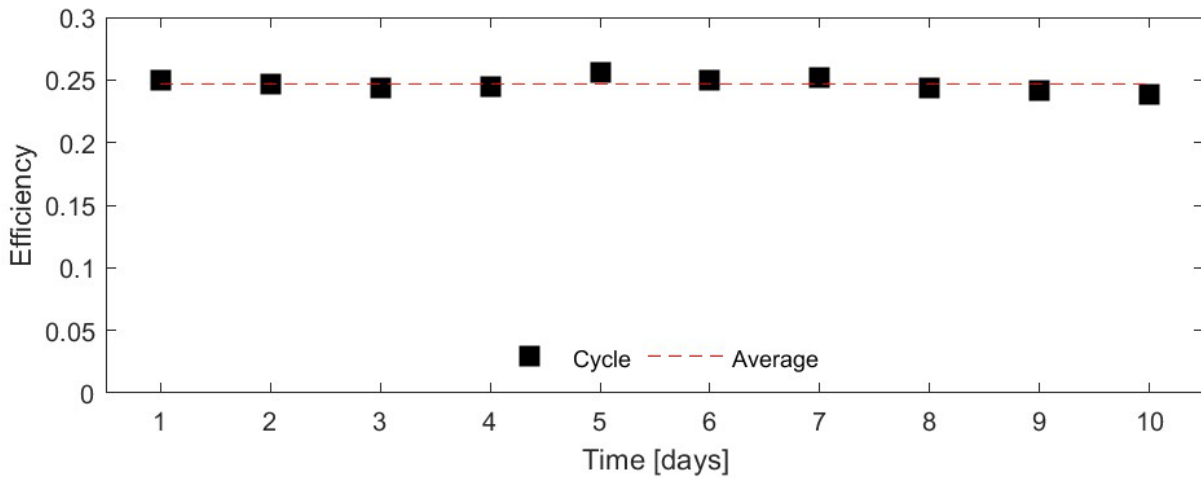
Figure 4. *TES.POD®'s power block efficiency for 10 consecutive days from Sep. 26th to Oct. 6th, 2022, at the KUMISP*

The TES.POD®'s electricity-to-electricity efficiency stands as the primary key performance indicator for assessing its performance throughout the testing phase. Figure 5 portrays charged and discharged energy alongside average, cumulative, and cycle efficiencies on a daily basis across the 10-day operational period. As efficiency is calculated through the ratio $E_{net,out}$ / $E_{net,in}$, it heavily relies on charge and discharge durations. The TES.POD®'s cycle efficiency ranges from 19% to 26.6%, averaging 23% over the testing timeframe. A comparison between the TES.POD® and other latent heat storage (LHS) technologies using Al-Si alloy-based PCM and a Stirling engine reveals the TES.POD® outperforms both tested STEALS prototypes and even exceeds optimistic expectations if STEALS were to be commercialized [17].
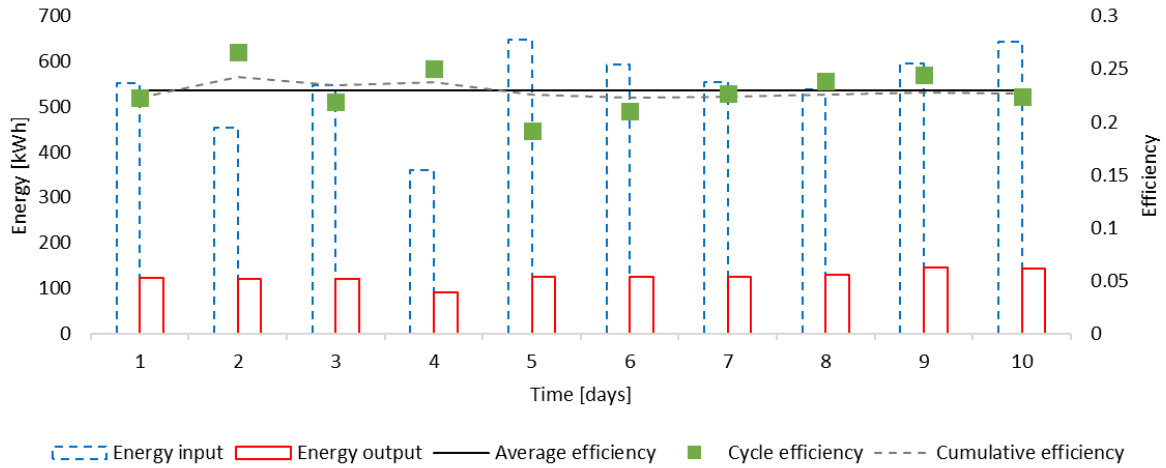
Figure 5. *TES.POD® daily net efficiency along with input and output energy for 10 consecutive days from Sep. 26th to Oct. 6th, 2022, at KUMISP*

6. Conclusions

Azelio's full-scale TES.POD® technology was successfully experimentally demonstrated at the KUMISP, indicating its potential for long duration energy storage applications. TES.POD® is a high-temperature latent heat storage solution that uses 88Al-12Si as a PCM, liquid sodium as a HTF, and Hydrogen as a working gas in the Stirling engine. Based on the experimental results obtained from the TES.POD®, the following conclusions may be drawn:

- TES.POD® charging takes around 6 hours at 90-100kW.
- TES.POD® has the ability to discharge the stored latent heat to generate electrical power between 9.5 and 11.5 kW over 13 hours.
- TES.POD® demonstrated an average net cycle electricity-to-electricity efficiency of 23%.

The results presented in this study, although promising, did not include the evaluation of the system heat losses, its performance in off-design operations (deep discharge) or its response time, which are important parameters for small grid stabilization. The techno-economic analysis, as well as the Life Cycle Assessment of the system, and the modelling of its inclusion in an electric grid were out of the scope of the project. Conversely, a post-mortem study of the system to determine the quality of the tank coating against corrosion by molten metal after hundreds of cycles was out the scope.

An extended article has been published in the Journal of Energy Storage in 2024, which included the off-design performance study, as well as the system's response time and heat losses [29]. Other aspects can be developed in subsequent works, in order to allow a proper benchmarking of this technology against other energy supply systems (i.e. diesel generators) or energy storage technologies (hydrogen, batteries, compressed air storage).

Data availability statement

The supporting data originates from the internal probes of the prototype, and is own by a third-party, the Swedish company Azelio, AB. As a result, sharing this data is restricted, and limited to only Khalifa University.

Author contributions

- Asem Alemam: data curation, formal analysis, investigation, visualization, writing – original draft
- Nicolas Lopez Ferber: conceptualization, methodology, supervision, writing-review and editing
- Tommy Malm: resources, investigation
- Valerie Eveloy: methodology, supervision, writing-review and editing
- Nicolas Calvet: project administration, funding acquisition, supervision, writing-review and editing

Competing interests

The authors declare that they have no competing interests.

Funding

Acknowledgement

References

[1]	Q. Hou, N. Zhang, E. Du, M. Miao, F. Peng, and C. Kang, "Probabilistic duck curve in high PV penetration power system: Concept, modeling, and empirical analysis in China," Appl Energy, vol. 242, no. March, pp. 205–215, 2019, doi: 10.1016/j.apenergy.2019.03.067.

[2]	M. W. Jack, A. Mirfin, and B. Anderson, "The role of highly energy-efficient dwellings in enabling 100% renewable electricity," Energy Policy, vol. 158, no. August, p. 112565, 2021, doi: 10.1016/j.enpol.2021.112565.

[3]	R. Shan, J. Reagan, S. Castellanos, S. Kurtz, and N. Kittner, "Evaluating emerging long-duration energy storage technologies," Renewable and Sustainable Energy Reviews, vol. 159, no. January, p. 112240, 2022, doi: 10.1016/j.rser.2022.112240.

[4]	M. Geyer, "Net-zero power; Long duration energy storage for a renewable grid," in Thermal-Mechanical-Chemical Energy Storage Workshop, 2022.

[5]	A. Gil et al., "State of the art on high temperature thermal energy storage for power generation. Part 1--Concepts, materials and modellization," Renewable and Sustainable Energy Reviews, vol. 14, no. 1, pp. 31–55, 2010.

[6]	V. Lebedev and A. E. A. Amer, "Thermal Energy Storage by Using Latent Heat Storage Materials," Int J Sci Eng Res, vol. 9, no. 5, pp. 1442–1447, 2018.

[7]   M. Opolot, C. Zhao, M. Liu, S. Mancin, F. Bruno, and K. Hooman, "A review of high temperature (≥ 500 °C) latent heat thermal energy storage," Renewable and Sustainable Energy Reviews, vol. 160, no. December 2021, 2022, doi: 10.1016/j.rser.2022.112293.

[8]   Y. Yuan, N. Zhang, W. Tao, X. Cao, and Y. He, "Fatty acids as phase change materials: A review," Renewable and Sustainable Energy Reviews, vol. 29, pp. 482–498, 2014, doi: 10.1016/j.rser.2013.08.107.

[9]   S. C. Costa and M. Kenisarin, "A review of metallic materials for latent heat thermal energy storage: Thermophysical properties, applications, and challenges," Renewable and Sustainable Energy Reviews, vol. 154, no. September 2021, p. 111812, 2022, doi: 10.1016/j.rser.2021.111812.

[10]   B. M. Diaconu, M. Cruceru, and L. Anghelescu, "A critical review on heat transfer enhancement techniques in latent heat storage systems based on phase change materials. Passive and active techniques, system designs and optimization," J Energy Storage, vol. 61, no. December 2022, p. 106830, 2023, doi: 10.1016/j.est.2023.106830.

[11]   G. Wei et al., "Selection principles and thermophysical properties of high temperature phase change materials for thermal energy storage: A review," Renewable and Sustainable Energy Reviews, vol. 81, no. May 2017, pp. 1771–1786, 2018, doi: 10.1016/j.rser.2017.05.271.

[12]   B. Cárdenas and N. León, "High temperature latent heat thermal energy storage: Phase change materials, design considerations and performance enhancement techniques," Renewable and Sustainable Energy Reviews, vol. 27, pp. 724–737, 2013, doi: 10.1016/j.rser.2013.07.028.

[13]   L. Qin et al., "Applying branch-shaped fins for improvement of performance of heat storage unit," J Energy Storage, vol. 55, no. PB, p. 105460, 2022, doi: 10.1016/j.est.2022.105460.

[14]   Y. Zheng et al., "Experimental and computational study of thermal energy storage with encapsulated NaNO3 for high temperature applications," Solar Energy, vol. 115, pp. 180–194, 2015, doi: 10.1016/j.solener.2015.02.002.

[15]   D. G. Gunjo, S. R. Jena, P. Mahanta, and P. S. Robi, "Melting enhancement of a latent heat storage with dispersed Cu, CuO and Al2O3 nanoparticles for solar thermal application," Renew Energy, vol. 121, pp. 652–665, 2018, doi: 10.1016/j.renene.2018.01.013.

[16]   N. Calvet, X. Py, R. Olivès, J. P. Bédécarrats, J. P. Dumas, and F. Jay, "Enhanced performances of macro-encapsulated phase change materials (PCMs) by intensification of the internal effective thermal conductivity," Energy, vol. 55, pp. 956–964, 2013, doi: 10.1016/j.energy.2013.03.078.

[17]   J. E. Rea et al., "Prototype latent heat storage system with aluminum-silicon as a phase change material and a Stirling engine for electricity generation," Energy Convers Manag, vol. 199, no. September, 2019, doi: 10.1016/j.enconman.2019.111992.

[18]   J. E. Rea et al., "Experimental demonstration of a dispatchable latent heat storage system with aluminum-silicon as a phase change material," Appl Energy, vol. 230, no. May, pp. 1218–1229, 2018, doi: 10.1016/j.apenergy.2018.09.017.

[19]   D. Laing, T. Bauer, D. Ehmann, and C. Bahl, "Development of a thermal energy storage system for parabolic trough power plants with direct steam generation," Journal of Solar Energy Engineering, Transactions of the ASME, vol. 132, no. 2, pp. 0210111–0210118, 2010, doi: 10.1115/1.4001472.

[20]   M. White, S. Qiu, and R. Galbraith, "Phase change salt thermal energy storage for dish stirling solar power systems," ASME 2013 7th Int. Conf. on Energy Sustainability Collocated with the ASME 2013 Heat Transfer Summer Conf. and the ASME 2013 11th Int. Conf. on Fuel Cell Science, Engineering and Technology, ES 2013, no. March 2015, 2013, doi: 10.1115/ES2013-18292.

[21]   S. Qiu, L. Solomon, and G. Rinker, "Development of an integrated thermal energy storage and free-piston stirling generator for a concentrating solar power system," Energies (Basel), vol. 10, no. 9, 2017, doi: 10.3390/en10091361.

[22]   Azelio, "Azelio Annual Report 2021," 2021.

[23]   A. Dindi, N. Lopez Ferber, D. Gloss, E. Rilby, and N. Calvet, "Compatibility of an Aluminium-Silicon metal alloy-based phase change material with coated stainless-steel containers," J Energy Storage, vol. 32, no. October, p. 101961, 2020, doi: 10.1016/j.est.2020.101961.

[24]   M. J. Assael, E. K. Mihailidou, J. Brillo, S. V. Stankus, J. T. Wu, and W. A. Wakeham, "Reference Correlation for the Density and Viscosity of Eutectic Liquid Alloys Al+Si, Pb+Bi, and Pb+Sn," J Phys Chem Ref Data, vol. 41, no. 3, 2012, doi: 10.1063/1.4750035.

[25]   S. Khare, M. Dell'Amico, C. Knight, and S. McGarry, "Selection of materials for high temperature latent heat energy storage," Solar Energy Materials and Solar Cells, vol. 107, pp. 20–27, 2012, doi: 10.1016/j.solmat.2012.07.020.

[26]   J. E. Rea et al., "Modular Concentrated Solar Power with Latent Heat Storage," Applied Energy (Supplementary information), 2018.

[27]   V. Sobolev, "Database of thermophysical properties of liquid metal coolants for GEN-IV," 2010.

[28]   M. Nilsson, A. Abou-Taouk, H. Sandberg, and J. Lindh, "A Stirling engine for thermal energy storage," in AIP Conference Proceedings, 2019. doi: 10.1063/1.5117653.

[29]   A. Alemam et al., "Experimental demonstration of a dispatchable power-to-power high temperature latent heat storage system," J Energy Storage, vol. 86, no. November 2023, 2024, doi: 10.1016/j.est.2024.111241.